

Capturing strong correlation effects on a quantum annealer: calculation of avoided crossing in the H_4 molecule using the quantum annealer eigensolver

Aashna Anil Zade,^{1,2,*} Kenji Sugisaki,^{1,3,4,5} Matthias Werner,^{6,7,8} Ana Palacios,^{6,7,8} Artur Garcia-Saez,^{6,9} Arnau Riera,⁶ and V. S. Prasanna^{1,10,†}

¹*Centre for Quantum Engineering, Research and Education, TCG CREST, Kolkata 700091, India*

²*Department of Physics, IIT Tirupati, Chindapalle, Andhra Pradesh 517619, India*

³*Graduate School of Science and Technology, Keio University, 7-1 Shinkawasaki, Saiwai-ku, Kawasaki, Kanagawa 212-0032, Japan*

⁴*Quantum Computing Center, Keio University, 3-14-1 Hiyoshi, Kohoku-ku, Yokohama, Kanagawa 223-8522, Japan*

⁵*Keio University Sustainable Quantum Artificial Intelligence Center (KSQAIC), Keio University, 2-15-45 Mita, Minato-ku, Tokyo 108-8345, Japan*

⁶*Qilimanjaro Quantum Tech, Carrer de Vençuela 76, 08019 Barcelona, Spain*

⁷*Departament de Física Quàntica i Astrofísica, Facultat de Física, Universitat de Barcelona, 08028 Barcelona, Spain*

⁸*Institut de Ciències del Cosmos, Universitat de Barcelona, ICCUB, Martí i Franquès 1, 08028 Barcelona, Spain.*

⁹*Barcelona Supercomputing Center, Pl. Eusebi Güell 1, 08032 Barcelona, Spain*

¹⁰*Academy of Scientific and Innovative Research (AcSIR), Ghaziabad- 201002, India*

(Dated: December 31, 2024)

We broaden the scope of the Quantum Annealer Eigensolver (QAE) algorithm, an underexplored noisy intermediate scale quantum (NISQ) era approach for calculating atomic and molecular properties, to predict avoided crossings, where strong correlation effects are at play. For this purpose, we consider the classic example of the H_4 molecule in a rectangular geometry. Our results are obtained on the 5000-qubit D-Wave Advantage system 4.1 quantum computer. We benchmark our quantum annealing results with full configuration interaction (FCI) as well as with those obtained using simulated annealing. We find that we can predict avoided crossings within about 1.1% of the FCI value on real quantum hardware. We carry out analyses on the effect of the number of shots, anneal time, and the choice of Lagrange multiplier on our obtained results. Since the QAE algorithm provides information on the wave function as its output, we also check the quality of the computed wave function by calculating the fidelity, and find it to be 99.886%. Finally, we qualitatively discuss the strengths and weaknesses of the QAE algorithm relative to its gate-based NISQ algorithm counterpart, the celebrated Variational Quantum Eigensolver. Our work contributes to the existing body of literature on QAE by demonstrating that high-quality results can be achieved on noisy hardware.

I. INTRODUCTION

Due to its general purpose nature, Quantum Annealer Eigensolver (QAE), which is a noisy intermediate scale quantum (NISQ) era quantum annealing algorithm [1] built on the variational principle, has been widely applied to a variety of problems. They include molecular vibrational spectra [1], complex eigenvalue problems [2], energy calculations for molecular electronic states [3, 4], relativistic calculations of fine structure splitting in highly charged atomic ions [5], simulating particle physics [6], and lattice gauge theories [7]. In one of these works,

the authors demonstrated that QAE could capture the fine structure splittings in highly charged atomic ions with unprecedented accuracy on quantum annealer hardware [5]. This aspect is especially noteworthy, since in gate-based NISQ hardware, noise poses significant problems, and thus obtaining results of comparable quality using similar approaches such as the variational quantum eigensolver (VQE) is extremely challenging. However, despite its general scope and better resilience to noise, the QAE algorithm has been vastly underexplored relative to VQE, which has received a lot of attention both on quantum hardware (for example, see Refs. [8–14] and simulation fronts (Refs. [15–22]).

The versatility and robustness of QAE to quantum hardware errors as well as dearth in the range of applications in the context of quantum chemistry naturally prompts further exploration of obtaining other molecular

* aashnazade@gmail.com

† srinivasaprasanna@gmail.com

properties using the algorithm. In particular, it is interesting and timely to study the performance of QAE in domains where predicting strong correlation effects, one of the cornerstones of quantum many-body theoretic calculations applied to quantum chemistry, are at play. This would be a first step towards mirroring the tremendous efforts that have been dedicated towards capturing strong correlation effects in the VQE framework [23–28].

In this work, we extend the range of applicability of the QAE algorithm into the strong correlation regime by carrying out avoided crossings (AC) calculations on the well-known prototypical system: H_4 in a rectangular geometry [29]. We expand the many-body wavefunction in a basis of configuration state functions (CSFs) and recast the energy functional as an Ising Hamiltonian. We then determine the ground state energy and the excited state energy of interest to us using three approaches: quantum annealing (for which we employ the QAE algorithm; on the D-Wave Advantage machine), simulated annealing (for which we use simulated annealing eigenvolver (SAE) approach), and the graphical unitary group approach full configuration interaction (GUGA-FCI; which we shall hereafter shorten to FCI for brevity) provided by GAMESS-US [30] for benchmarking our results. We also carry out an analysis of the ‘knobs’ of the QAE algorithm, such as the effect of the number of shots, the anneal time, and the choice of the Lagrange parameter on our AC results. Finally, since QAE and VQE are both NISQ algorithms, we compare the two approaches.

The rest of the sections are organized as follows: Section II presents the relevant theory and methodology, while Section III discusses our findings. In Section IV we compare QAE with VQE and conclude with Section V.

II. THEORY AND METHODOLOGY

A. Quantum annealing

QA is a meta-heuristic that leverages quantum fluctuations, and is designed to solve computationally hard optimization problems, typically by encoding them into the ground state of a Hamiltonian [31–33]. The underlying principle behind QA is the adiabatic theorem. Originally proposed by Born and Fock in 1928 [34], the adiabatic theorem can be encapsulated as follows: Given a time-dependent Hamiltonian, $H(t) = \left(1 - \frac{t}{T}\right)H_I + \frac{t}{T}H_F$; $t \in [0, T]$, which is initially H_I at $t = 0$ and subsequently H_F at some later time, $t = T$, and given that the system starts in the ground state of H_I , the state of the system

is guaranteed to remain in the ground state throughout its time evolution as long as the Hamiltonian is varied sufficiently slowly. Thus, the state of the system is in the ground state of H_F at $t = T$. QA involves preparing the ground state of an easily constructible Hamiltonian, H_I , which is typically chosen to be the transverse field Hamiltonian, and then gradually transforming it into another Hamiltonian, H_F , generally chosen to be the Ising Hamiltonian whose ground state encodes the solution to the problem. As one gradually goes from H_I to H_F , the system transitions smoothly from the ground state of H_I to the ground state of H_F . Since QA is naturally suited to finding global minima of energy landscapes, we use it to obtain the ground state energies of electronic structure Hamiltonians, which are expressed in the Ising form. We use the QAE algorithm for this purpose [1].

B. The QAE algorithm: a primer

The QAE algorithm solves the eigenvalue equation $H|\Psi\rangle = E|\Psi\rangle$ by transforming it into an energy minimization problem. The energy functional considered is the expectation value of the Hamiltonian H with respect to the unknown state $|\Psi\rangle$. To avoid trivial solutions, the normalisation constraint $\langle\Psi|\Psi\rangle - 1 = 0$ is enforced by the inclusion of a Lagrange multiplier λ into the energy functional. The modified formulation after dropping the irrelevant constant is given by

$$\epsilon = \langle\Psi|H|\Psi\rangle - \lambda\langle\Psi|\Psi\rangle. \quad (1)$$

Assuming an ansatz of the form $|\Psi\rangle = \sum_{i=1}^N c_i |\Phi_i\rangle$ where $\{|\Phi_i\rangle\}$ represent a set of N known basis functions, the QAE algorithm aims to determine the unknown coefficients $\{c_i\}$ with $c_i \in [-1, 1]$. These coefficients are encoded into K bits using the fixed point encoding scheme. This approach converts the problem from a continuous optimization over the variables $\{c_i\}$

$$\epsilon(\vec{c}, \lambda) = \sum_{i,j=1}^N c_i c_j H_{ij} - \lambda \sum_{i=1}^N c_i^2. \quad (2)$$

into a discrete optimization problem over the binary variables $\{q_i\}$ where $q_i \in \{-1, 1\}$ making it suitable for implementation on modern day quantum annealers. In the above equation, H_{ij} refers to the matrix elements of the Hamiltonian.

The pseudocode below summarizes the QAE implementation.

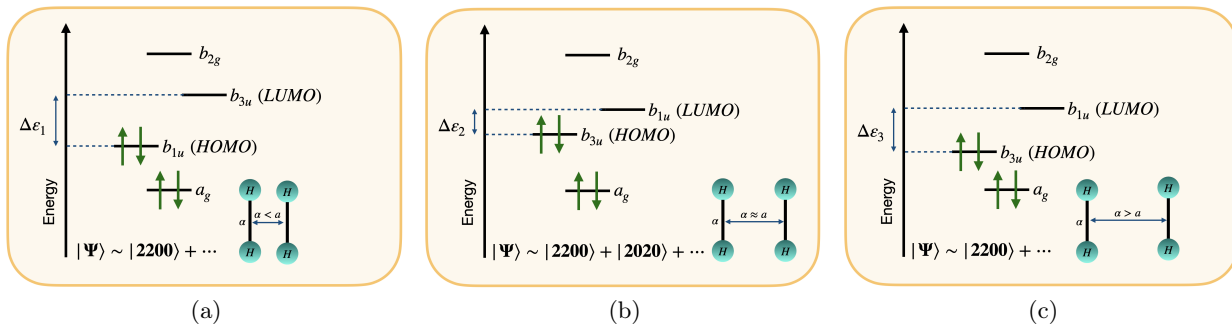


Figure 1: Molecular orbital diagram for H_4 across its potential energy curve, for the cases (a) $\alpha < a$, (b) $\alpha \approx a$, and (c) $\alpha > a$, where α denotes the distance between two H_2 sub-systems that constitute H_4 , whereas a is the bond length of the H_2 molecule. In the sub-figures, a_g , b_{1u} , etc refer to the irreducible representations of the D_{2h} point group, while $\Delta\epsilon_i$ is the difference in energy between the HOMO and LUMO across the PEC. HOMO and LUMO are the highest occupied and the lowest unoccupied molecular orbitals respectively.

Algorithm: QAE

```

Get  $H$ , Guess  $\lambda_{\pm}$ 
for  $\lambda \in [\lambda_-, \lambda_+]$  do
   $\epsilon(\vec{q}, \lambda) \leftarrow \epsilon(\vec{c}, \lambda)$  ▷ Encoding
   $\vec{q}_{\text{optimum}} \leftarrow [\epsilon(\vec{q}, \lambda)]_{\text{min}}$  ▷ Annealing
   $\vec{c}_{\text{optimum}} \leftarrow \vec{q}_{\text{optimum}}$  ▷ Reverse encoding
   $E_{\lambda} \leftarrow \epsilon(\vec{c}_{\text{optimum}}, \lambda)$ 
end for
Get  $\min\{E_{\lambda}\}$ 

```

In the succeeding paragraphs, we describe the theory behind avoided crossings, followed by details on obtaining them in the QAE framework.

C. Avoided crossings

An accurate description of ground and excited state potential energy curves (PECs) in regions where the electronic states interact strongly poses a challenge for well-known electronic structure methods such as the single reference coupled cluster approach [35–38]. These strongly interacting regions, termed as avoided crossings, involve geometries far from equilibrium where an accurate description of the electronic structure requires accounting for both strong and weak correlation effects, of which the former are predominant. In fact, ACs are a key indicator of strong correlation effects wherein the Hartree–Fock (HF) state alone no longer acts as a good reference for methods such as coupled cluster to compute accurate wavefunctions.

In the case of H_4 , this behaviour originates from the quasi-degenerate nature of the molecular orbitals, which

can be continuously varied by changing the parameter that defines the geometry, α . The parameter corresponds to the distance between the two H_2 sub-systems, each with bond distance separation given by a . Specifically, when $\alpha \neq a$, the energy gap between the highest occupied molecular orbital (HOMO) and the lowest unoccupied molecular orbital (LUMO) is substantial. This makes the HF configuration, given by $|2200\rangle$ in the occupancy number representation (specification of the occupancy of each orbital), dominant such that $|\Psi\rangle_{\alpha \neq a} \sim |2200\rangle$, thus enabling single reference methods to accurately describe the wavefunction in these regions. Conversely, when $\alpha \approx a$, the HOMO and LUMO become nearly degenerate and an additional configuration $|2020\rangle$ begins to contribute significantly alongside HF resulting in $|\Psi\rangle_{\alpha \approx a} \sim |2200\rangle - |2020\rangle$. Figure 1 depicts the orbital degeneracies along varying parameter values. The ‘ \sim ’ symbol is to indicate that we are ignoring the normalization constants for brevity, whereas the ‘ \dots ’ symbol indicates that the rest of the states besides those mentioned on the right hand side do not contribute significantly.

The AC in H_4 can also be understood from a group theoretic point of view. The non crossing rule put forth by Neumann and Wigner in 1929 [39] states that PECs corresponding to electronic states of same point group symmetry do not cross. Formally symmetry of an electronic state can be determined by evaluating the direct product of the irreducible representation of each of the electrons involved in that state. For H_4 , this corresponds to the A_g symmetry of the D_{2h} point group.

ACs are significant in quantum chemistry for studying reaction dynamics. They often correspond to the energy

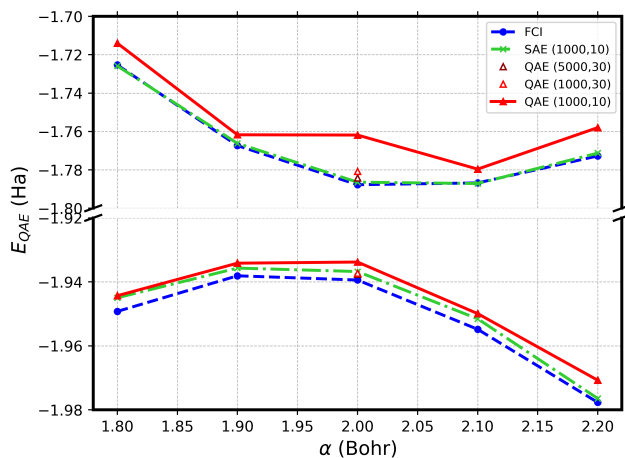


Figure 2: Comparison of the potential energy curves of the ground electronic state (singlet) and the first excited electronic state (singlet) obtained for H_4 for different values of α , using FCI, SAE, and QAE (on the D-Wave hardware). We calculate all of the data points with 1000 shots and 10 repetitions (denoted in the legend as (1000,10)), and setting an anneal time of 20 microseconds. The red and brown hollow triangle markers indicate our results obtained with 1000 shots and 30 repetitions (denoted in the legend as (1000,30)) and with 5000 shots and 30 repetitions (denoted in the legend as (5000,30)) respectively.

of transition states in chemical reactions. By accurately determining the energy at an AC, we can identify the major reaction pathway among multiple possible transition states. In this work, we use QAE to predict ACs in the H_4 molecule. The primary source of avoided crossing arises from the symmetry of the electronic states. Additionally, this model system allows us to vary the degree of orbital quasi-degeneracies by simply changing the geometry defining parameter.

D. Computational details

We begin by detailing the input parameters associated with our chosen molecule. H_4 is a planar four-electron model consisting of two interacting hydrogen molecules. The geometry is defined by intermolecular and intramolecular H...H distances α and a respectively, where the latter is fixed to 2 Bohr. We calculate the ground and excited state energies at five geometries (α

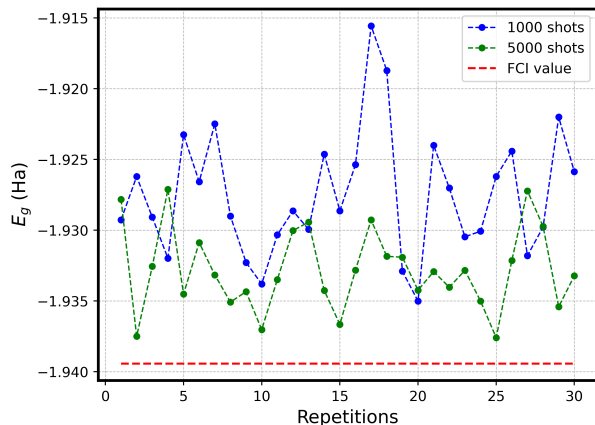


Figure 3: Comparison of the ground state energy at the AC geometry obtained by executing QAE (on the D-Wave hardware) with 1000 shots and 30 repetitions (marked in blue) and 5000 shots and 30 repetitions (marked in green). The reference FCI value is presented as a dashed line.

$= 1.8, 1.9, 2.0, 2.1, \text{ and } 2.2$ Bohr; for the purposes of this work, we fix the resolution to 0.1 Bohr in view of the cost of quantum computational resources). We work with the STO-3G minimal basis set and employ the D_{2h} point group symmetry in our calculations.

To generate the molecular Hamiltonian, we use the GUGA-FCI approach available in the GAMESS-US program [30]. There are 8 CSFs for our 4 electron 4 orbital active space. This corresponds to an 80×80 all-to-all connected QUBO problem with $K = 10$.

We now comment on the computational details in the QAE part of our workflow. We use the D-Wave Advantage system 4.1 for all the QAE computations. We need to choose a range of λ values across which we scan. For this purpose, we first carry out several SA computations, each with a different choice for the λ range. A given λ range is subdivided into 1000 parts, and for each of those λ values, we carry out SAE (the approach involves all of the steps from QAE, except that the quantum annealing is replaced by simulated annealing) with 1000 shots. We pick that λ range for our QAE calculation that gives the best energy value. All of our SAE calculations are performed using the D-Wave Ocean Toolkit [40]. For our QAE calculations, we subdivide the chosen λ range into 100 values, and perform QA with 1000 shots for each of those λ values. For each anneal, we pick the default anneal time of 20 microseconds. Once we find the lowest energy from the procedure, we repeat the process 10 times (we term this as 10 repetitions hereafter) and choose the

lowest energy among the set of values for our final result for the ground state energy. We note that for an excited state calculation, we follow the same procedure, except that the Hamiltonian, H_e , is constructed from the ground state Hamiltonian, H_g , and the ground state wave function, $|\Psi_g\rangle$, by invoking the Brauer’s theorem as

$$H_e = H_g + S_0 |\Psi_g\rangle \langle \Psi_g|.$$

This theorem states that the lowest eigenvalue of H_e corresponds to the second-lowest eigenvalue of H_g , which represents the first excited state energy we are looking for. Here, $S_0 > E_e - E_g$. We choose S_0 to be 1 in our work.

III. RESULTS AND DISCUSSIONS

We now discuss our results. Figure 2 presents our main result (with accompanying data provided in Table I), where we compare the predicted avoided crossing from QAE with SAE and FCI, with 1000 shots and 10 repetitions. From the figure, we see that QAE, SAE, and FCI yield an energy difference (at the AC geometry, that is, 2 Bohr) of 0.17195, 0.15037, and 0.15169 Hartree (Ha) respectively. Thus, QAE is able to predict AC in the chosen system to within about 13 percent of the FCI value. The plot also shows that SAE is clearly in better agreement with the FCI values than QAE with both the ground and excited state energies at all of the geometries considered. Furthermore, the quality of the predicted excited state energy is relatively poor for the AC geometry using QAE (as we shall discuss later, the quality of results from QAE is still substantially better than those from a VQE computation with the same parameters). We can backtrack the performance of QAE to the several input parameters that go into obtaining a QAE result, such as (but not limited to) the number of shots and number of repetitions, anneal time, and choice of λ range. We devote the subsequent paragraphs to analyzing the effect of these three parameters on the AC results.

We begin by carrying out AC calculations with 1000 shots and 30 repetitions. As Figure 2 shows, increasing the number of repetitions drastically improves the quality of the excited state energy (the difference with respect to the FCI value) improves from 25.8 mHa to 7 mHa and improves the agreement of the ground state energy with the FCI value to 4.4 mHa (from 5.6 mHa). The AC value improves from 20.2 mHa for 10 repetitions to 2.6 mHa for 30 repetitions. We extend the analysis further by increasing the number of repetitions all the way to 100, but find that the AC value remains unchanged. Thus, we instead

Table I: Table presenting data (with 1000 shots and across 10 repetitions) on the percentage accuracies of the ground state (\mathcal{A}_g) and excited state energies (\mathcal{A}_e) as well as the avoided crossings (\mathcal{A}_{AC}) for the geometries considered for this work, all of them relative to their respective FCI values. The fourth row gives results with 1000 shots and 30 repetitions at the AC geometry, whereas the last row presents results with 5000 shots and across 30 repetitions (only at the AC geometry). The geometries are specified by α in units of Bohr. The entries shown in parentheses for the AC geometry indicates the difference between that energy and its FCI counterpart (in units of mHa).

Shots	α	\mathcal{A}_g	\mathcal{A}_e	\mathcal{A}_{AC}
	1.8	99.75	99.34	102.87
	1.9	99.80	99.68	100.98
1000	2.0	99.71 (5.6)	98.55 (25.8)	113.35 (20.2)
		99.89 (4.4)	99.61 (7.0)	103.20 (2.6)
	2.1	99.75	99.60	101.36
	2.2	99.65	99.17	103.81
5000	2.0	99.91 (1.83)	99.80 (3.55)	101.14 (1.72)

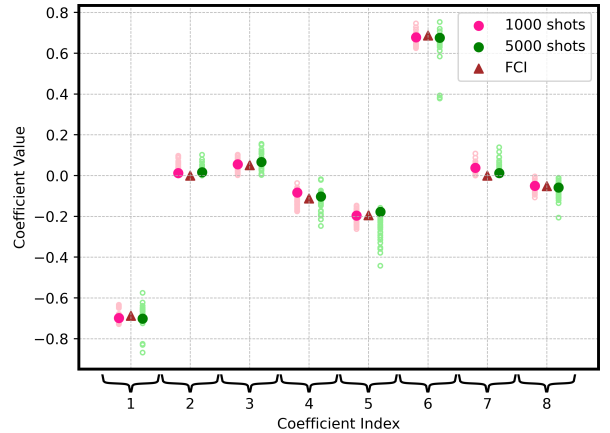


Figure 4: Comparison of CI coefficients for the ground state obtained using QAE with exact values of the coefficients from FCI (denoted as a brown triangle) for 1000 and 5000 shots, both with 30 repetitions, at the AC geometry. Each of the pink (1000 shots) and green (5000 shots) circles denotes the result from a repetition.

increase the number of shots to 5000 while keeping the number of repetitions fixed at 30. Figure 3 presents our findings, with the accompanying data given in Table I. The results indicate that as expected, one obtains better agreement with the FCI value for the AC with larger num-

ber of shots and repetitions. Furthermore, we see that the QAE result now is in much better agreement with the FCI value, differing only by 1.14 percent (5000 shots, 30 repetitions), as opposed to the 1000 shots 10 repetitions value of 13.35 percent and the 1000 shots 30 repetitions value of 3.2 percent. These percentages correspond to an energy difference ($E_{AC,FCI} - E_{AC,QAE}$) of 1.72 mHa, 20.2 mHa, and 2.6 mHa respectively. The values of AC obtained with 5000 shots and 30 repetitions, 1000 shots and 10 repetitions, and 1000 shots and 30 repetitions are 0.15342, 0.17195, and 0.15654 Ha respectively.

We turn our attention to Figure 4, where we plot the CI coefficients that we obtained from the ground state QAE calculation versus the coefficient index. We benchmark the computed CI coefficients employing QAE with those obtained from FCI. We carry out the exercise for both the 1000 and the 5000 shot cases, each with 30 repetitions. The purpose of the plot is to check the quality of the coefficients, which in turn indicates the quality of the predicted wave function. We see that the coefficients are all in reasonable agreement with their FCI counterparts. While the plot itself seems to yield almost similar set of coefficients by using 5000 shots over 1000 shots, this seemingly insignificant difference between their results is reflected in the subsequent ground state energy calculations as seen in the preceding paragraphs. Unsurprisingly, we also see the chemistry at play, where two coefficients are almost equally important (unlike the single reference scenario where only the HF state dominates). We also check the fidelity as well as the difference between AC predicted using QAE and FCI, and find them to be 99.735% and 2.6mHa respectively for QAE calculation with 1000 shots and 30 repetitions, whereas they improve to 99.886% and 1.72 mHa respectively when we employ 5000 shots and 30 repetitions. Figure 5 presents scatter plots between fidelity (\mathcal{F}) and ΔE , the difference between the QAE and the FCI ground state energy results. The fidelity is given by $|\langle \Psi_{QAE} | \Psi_{FCI} \rangle|^2$, where $|\Psi_{QAE}\rangle$ is the wave function constructed using the CI coefficients that QAE outputs, while $|\Psi_{FCI}\rangle$ refers to the FCI wave function. We carry out linear regression analysis on our two data sets, and find that the Pearson coefficient, R , is weakly correlated (0.115) for the 1000 shots case but is weakly anti-correlated (-0.22) in the 5000 shots scenario. Ideally, we would expect that as we supply more shots, the strength of anti-correlation between the two quantities, \mathcal{F} and ΔE , increases, based on the inequality $\mathcal{F} \geq 1 - \frac{\Delta E}{E_{AC,true}}$, where $E_{AC,true}$ is the FCI value for the energy at the AC. Our data supports this expectation. Furthermore, we find the best-case fidelities and ground state energies that we obtain using QAE for both the 1000 and the 5000 shots cases (99.735% and 99.886%

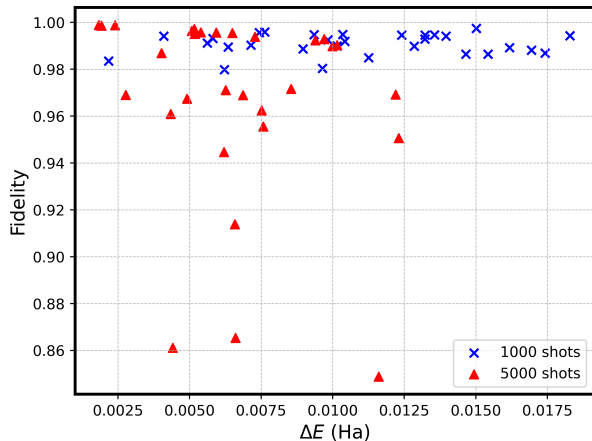


Figure 5: Scatter plot involving fidelity and ΔE values. The former quantity refers to $|\langle \Psi_{QAE} | \Psi_{FCI} \rangle|^2$, where $|\Psi_{QAE}\rangle$ is the wave function constructed out of the CI coefficients obtained using QAE and $|\Psi_{FCI}\rangle$ is the FCI wave function. On the other hand, the latter is the difference between the QAE and the FCI ground state energy results.

respectively) obey the aforementioned inequality relation.

We now comment on the effect of anneal time on our results. We begin by recalling that the Hamiltonian changes for the ground and excited states, and thus our assumption of setting the same anneal time for the ground and excited state computations is simplistic. Figure 6 presents our results for the variation of the ground state energy E_g , the excited state energy E_e , and AC with anneal time, with the purpose of going beyond the assumption that we had made in our main results shown in Figure 2. We choose to carry out the study with anneal times chosen between 10 and 40 microseconds. We carry out a coarse grained analysis in the interest of computational cost, and with unequal time resolutions across this range so that we probe with smaller resolution in and around the default anneal time of 20 microseconds. We use 1000 shots and 10 repetitions for the analysis. The plot shows that the default time happens to yield particularly poor results for the excited state relative to the other values of anneal time. If we instead pick the anneal times that give the best results for the ground state and excited state energies, the AC value improves from 0.17195 Ha to 0.15201 Ha. In the interest of computational cost, we did not carry out the analysis for the case of 5000 shots and 30 repetitions, but we anticipate to obtain further improvement in the AC energy value with this approach.

Finally, we focus on the choice of λ range for the prob-

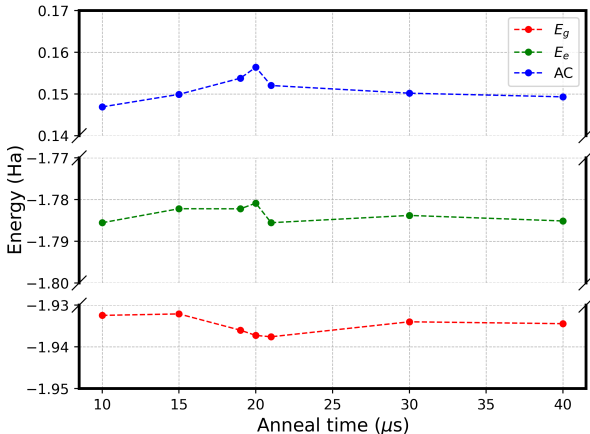


Figure 6: Plot showing the ground state energy (E_g), excited state energy (E_e), and avoided crossing (AC) values for different anneal times (in microseconds). The calculations are carried out with 1000 shots and 10 repetitions.

lem. As mentioned in an earlier paragraph in Section II, we picked the λ range that gave the best SAE result. For the purposes of this work, we pick a range of 0.1 Ha. However, since SAE and QAE are different approaches to search for a desired solution, we pick three such ranges of 0.1 Ha each: a range containing the HF value (-1.77 Ha), which is -1.8 to -1.7 Ha, one that is immediately below and another that is immediately above it. We term the three ranges as A, B, and C respectively. We note that the range we picked for our main calculations was the one immediately *above* the HF value, that is, range C. Figure 7 presents our results justifying this choice. We observe that our choice of λ range from SAE calculations were sufficiently good within a calculation involving 30 repetitions.

IV. COMPARISON OF QAE AND VQE

We devote this section to a qualitative comparison of the strengths and weaknesses of VQE, the leading NISQ algorithm for quantum chemistry, and the QAE algorithm. We add that we do not compare the performance of QAE with best known classical computing algorithms, since it is a NISQ approach, and a comparison with VQE is likely more suitable in that context. It is worth noting that we do not, for the purposes of the qualitative analysis, compare QAE with variants of VQE, but with only the traditional version of the latter.

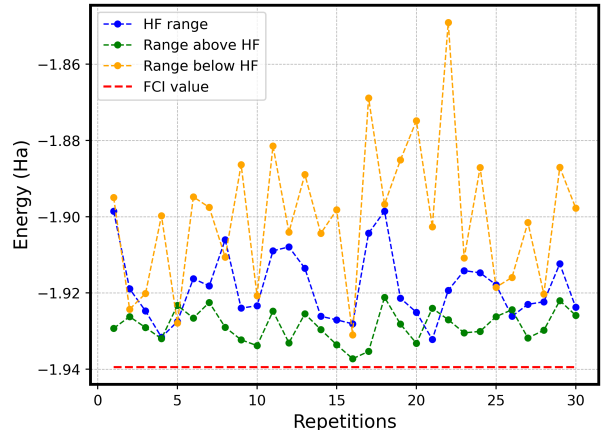


Figure 7: Comparison of the ground state energy across the three different λ ranges considered. The FCI value of the ground state energy is provided for reference as a dashed line.

We begin with general remarks on both the algorithms, before we discuss results from our numerical calculations of AC using the VQE algorithm.

- The very first consideration is the absence of gates in QAE. Since gate errors are a major limiting factor in gate-based approaches of which VQE is one, the accuracy in results that one expects from a gate-based algorithm is usually limited, as opposed to approaches involving quantum annealing. The results from Ref. [5], where the authors achieve an accuracy of about 99 percent, indeed reflects this observation.
- We also note that QAE possesses another inherent advantage in giving better results, since we pick the lowest energies across repetitions by construction. This is in contrast to VQE, where the mean expectation value across repetitions is typically chosen as the final result.
- Furthermore, in VQE, the choice of ansatz is paramount. While physics-inspired/chemistry-based ansätze such as the unitary coupled cluster (UCC) based ones yield excellent results in noiseless simulations, the entire class of hardware efficient ansätze often suffer from the notorious barren plateau problem. On the other hand, we are unlikely to run into barren plateau issues in QAE, since by construction, we employ a CI wave function, which is physics-inspired/chemistry-based, and the algorithm involves an explore-exploit

metaheuristic strategy, due to which we do not have a notion of iterations and convergence. It is worth adding that modified QAE workflows could have a convergence aspect to it, for example, see Ref. [5], but in our current study, we use the originally proposed QAE workflow, where we simply execute many shots of quantum annealing for each pre-selected λ value within a range.

- This also leads us to the next point: since VQE is iterative in nature, the convergence behaviour heavily relies on the choice of optimizer (with the correct choice not being necessarily easy), the precision sought, as well as the nature of the specific system of interest. On the other hand, one can think of quantum annealing itself as performing the optimization in the case of QAE.
- The number of parameters to optimize grow identically for both UCC-based VQE and QAE (which relies on CI). For example, in a UCCSD (UCC in the singles and doubles approximation) ansatz-based VQE computation, the number of parameters to be optimized grow as $\sim n_o^2 n_v^2$, where n_o and n_v refer to the number of occupied and unoccupied spin orbitals respectively. The number of parameters to optimize in QAE also grows identically for CISD (configuration interaction in the singles and doubles approximation).
- The inputs to VQE are the one- and two-electron integrals. The inputs to QAE are the CI Hamiltonian (which in turn require one- and two- electron integrals) and also λ . The requirement of finding the latter adds an additional layer of complication to QAE.
- We now move to the range of physical effects that the two approaches can capture. VQE-UCCSD, in its traditional form, is not suited to handle strong correlation effects of the type we address in this work, whereas QAE, which is based on CI, is. If VQE needs to address strong correlation effects, we need to employ suitable variants such as a multi-reference UCC (MRUCC) ansatz, which is typically accompanied by more quantum resources, or alternatives such as use of a double exponential UCC-like ansatz [41], etc. We also add here that comparing UCCSD-based VQE and FCI-based QAE is reasonable, especially since we are dealing with a small system in our work, and thus the difference in the quality of correlation effects captured by UCCSD and FCI are not as critical for the purposes of the analysis.

- Both algorithms face some common challenges, such as the lack of a fully connected hardware can lead to incurring more quantum resources (more CNOT gates for VQE via SWAP gates, and more physical qubits for QAE via embedding). There exist some fully connected gate-based computers (for example, IonQ Aria and Forte devices, as well as the Quantinuum Model H1 and H2 machines), but we are yet to have such an annealing hardware (although work is underway on architectures such as the LHZ type [42]).
- QAE also has the drawback of current QA hardware only being able to accommodate the transverse field Ising Hamiltonian, thus leading to encoding costs.

We now carry out the AC calculation in the VQE framework. We first calculate the ground state energy, followed by computing the excited state energy of interest to us in the quantum equation of motion VQE framework. We pick the AC geometry (2 Bohr). We use the Qiskit 1.3.1 package [43] throughout. We carry our 8-qubit, 26-parameter, noiseless VQE simulations with 1000 shots, and across 10 repetitions, we obtain a mean energy of -1.93288 Ha for the ground state energy. We recall that with 1000 shots and 10 repetitions, QAE, on the D-Wave hardware, yields a lower energy of -1.93381 Ha. As Fig. 8 shows, the mean energy obtained from a noiseless VQE simulation improves to -1.93875 Ha upon increasing the number of shots to 5000, which is better than the QAE estimate with 1000 shots and 10 repetitions. We note that the value is better than those obtained from QAE with 5000 shots and 10 repetitions (-1.93750 Ha) and with 5000 shots and 30 repetitions (-1.93760 Ha). We recall that the FCI value is -1.93943 Ha. Lastly, since VQE employs a single reference UCCSD ansatz, the results are obtained at the cost of slow convergence. The computation took 298 iterations to converge with the SLSQP optimizer, in contrast to 168 iterations that it took for convergence at 1.2 Bohr geometry and 113 at the 8 Bohr geometry, where strong correlation effects are less pronounced. A similar observation on a single reference ansatz yielding reasonable results at the cost of more iterations was observed in Ref. [13]. Our Quantum Equation of Motion (QEOM) state vector calculations [44] *directly* predicted an AC value of 0.14578 Ha (the excited state energy was -1.79250 Ha), which is within about 4 percent of the FCI AC value.

In order to place the QAE and VQE computations on an equal footing, we would also need to compute the ground state energy using VQE on real quantum hardware. We do not carry out such a calculation here, but

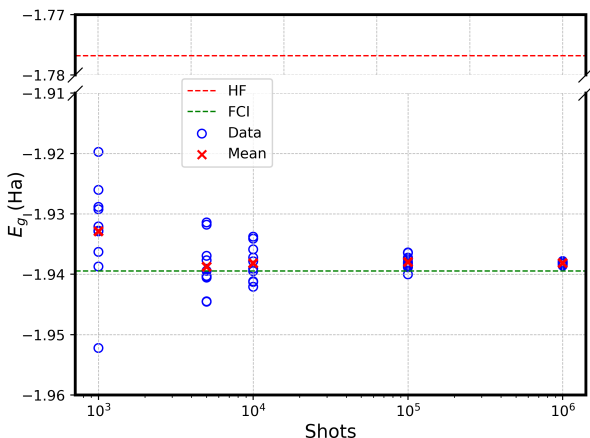


Figure 8: Comparison of the ground state energy (E_g) obtained using VQE across different number of shots. For each shot number, we repeat the VQE calculation 10 times (10 repetitions). The HF and the FCI values are provided for reference.

assess the challenges that we anticipate in such a scenario. Assuming that we carry out the calculation on the IBM Brooklyn device, we incur 2244 CX gates (the number of one-qubit gates are 3200, 1216, and 4 for RZ , SX , and X respectively). We note that even if the device had been fully connected, the number of two-qubit gates is still 1440, which would yield a rather low result fidelity. For example, assuming an optimistic estimate of 0.999 for the two-qubit gate fidelity, an estimate of the result fidelity even with a fictitious all-to-all connected topology is a mere $\sim 0.999^{1440} \approx 0.2$. Thus, in order to obtain meaningful results, one needs to aggressively optimize the quantum circuit in addition to implementing additional resource reduction strategies to reduce the number of measurements, etc [22]. The authors show in Ref. [22] that with a suite of such classically resource-intensive strategies, the number of gates can be reduced to the extent that makes computation on current-day quantum devices possible.

V. CONCLUSION AND FUTURE OUTLOOK

In summary, we carry out calculations to predict an avoided crossing in the H_4 molecule on a D-Wave quantum computer. The motivation for this work is two-fold: first, to address the challenge of capturing strong correlation effects, which are widely regarded as a cornerstone of physical chemistry, and second, to bridge a significant

gap in literature with regard to the application of quantum annealers to NISQ-era chemistry, in contrast to the extensive body of research dedicated to the gate-based VQE algorithm in the same domain. We find from our calculations that using the QAE algorithm with 1000 shots and 10 repetitions yields AC with reasonable precision, to within about 20 percentage of the reference full configuration interaction values. Furthermore, we find that the result can be improved by increasing the number of shots to 5000, the number of repetitions to 30, and by choosing different anneal times for the ground and excited state energies. The choice of λ range using SAE was sufficient. The improved AC result with 5000 shots and 30 repetitions is to within about 1.1 percent of the FCI value. Among the factors considered, we find that unsurprisingly, the number of shots significantly influences the quality of our results. It is also worth noting at this point that there are several other factors that could be tuned to improve the results further, which we do not carry out in this pilot study. These include, but are not limited to:

- Checking the effect of including more λ values within a chosen λ range.
- Checking the effect of the number of physical qubits that are expended for a computation via embedding. We find that for a given repetition, that is, across hundred λ values that are scanned for our chosen λ range, the number of physical qubits can vary between about 700 to about 900 to construct our QUBO with 80 logical qubits. It is important to note that embedding is a heuristic, and it is worth exploring this direction further to improve the quality of results.
- A study of the dependence of results on K . This is fairly non-trivial in practice, since for a Hamiltonian matrix of size N , an increase in K (to achieve better precision in the CI coefficient values) leads to corresponding all-to-all connected QUBO growing as NK . While embedding larger graphs would likely incur more error, an acute problem that one would face is running out of physical qubits. For example, were we to carry out the same computations on H_4 with a split valence basis set such as the 6-31G (4 electron- 5 orbital active space), a QUBO size of 170 (assuming $K = 10$) requires on an average about 4000 physical qubits (over those scanned λ values for which an embedding was found). Finding an embedding with any further increase in K is not possible, since the D-Wave annealers have only 5000 physical qubits. In such cases, one needs to opt for

Sub-QUBOs (for example, see Ref. [45]), and additional errors incurred in approximations involved in choice of sub-QUBOs also add to the error budget. It is worth adding that the embedding issue we consider is specific to current state-of-the-art D-Wave hardware and not to the QAE algorithm itself; future advances in this direction, for example, machines with substantially better connectivity, could alleviate embedding-related issues.

- Our calculations are spread over a time period of about three months, and thus we expect that our results and analyses would have errors due to drift in machine parameters. It is, however, well beyond the scope of the current study to address the issue.

We also carry out a qualitative comparison of the QAE algorithm with the celebrated VQE approach, and find that while both methods have their own pros and cons, QAE is a compelling NISQ-era contender for quantum chemistry on quantum computers.

We anticipate that our study paves way for more comprehensive and detailed studies on the underexplored QAE algorithm, and also for algorithmic advances in

NISQ approaches for quantum chemistry in the quantum annealing framework.

ACKNOWLEDGMENTS

This work was supported by the European Commission EIC-Transition project RoCCQeT (GA 101112839). AAZ and VSP sincerely acknowledge Palak Chawla for her tremendous support and patience in helping us with the VQE computations, and Disha Shetty for patiently reading the initial drafts and giving her feedback, which in turn helped improve the quality of the manuscript. VSP and AAZ acknowledge Prof. Bhanu Pratap Das for discussions on QAE and support with D-Wave time, and Prof. Debashis Mukherjee for discussions on the general nature of AC. The authors acknowledge Mr. Jose Miralles for fruitful discussions on Sub-QUBOs. KS acknowledges support from Quantum Leap Flagship Program (Grant No. JPMXS0120319794) from the MEXT, Japan, Center of Innovations for Sustainable Quantum AI (JPMJPF2221) from JST, Japan, and Grants-in-Aid for Scientific Research C (21K03407) and for Transformative Research Area B (23H03819) from JSPS, Japan.

-
- [1] A. Teplukhin, B. K. Kendrick, and D. Babikov, *J. Chem. Theory Comput.* **15**, 4555 (2019).
- [2] A. Teplukhin, B. K. Kendrick, and D. Babikov, *Phys. Chem. Chem. Phys.* **22**, 26136 (2020).
- [3] A. Teplukhin, B. K. Kendrick, S. Tretiak, and P. A. Dub, *Sci. Rep.* **10**, 20753 (2020).
- [4] A. Teplukhin *et al.*, *Sci. Rep.* **11**, 18796 (2021).
- [5] V. Kumar, N. Baskaran, V. S. Prasanna, K. Sugisaki, D. Mukherjee, K. G. Dyllal, and B. P. Das, *Phys. Rev. A* **109**, 042808 (2024).
- [6] M. Illa and M. J. Savage, *Phys. Rev. A* **106**, 052605 (2022).
- [7] S. A. Rahman, R. Lewis, E. Mendicelli, and S. Powell, *Phys. Rev. D* **104**, 034501 (2020).
- [8] A. Peruzzo *et al.*, *Nat. Commun.* **5**, 4213 (2014).
- [9] A. Kandala, A. Mezzacapo, K. Temme, M. Takita, M. Brink, J. M. Chow, and J. M. Gambetta, *Nature* **549**, 242 (2017).
- [10] F. Arute *et al.*, *Science* **369**, 1084 (2020).
- [11] Y. Nam *et al.*, *Npj Quantum Inf.* **6**, 33 (2020).
- [12] C. Ying *et al.*, *Phys. Rev. Lett.* **130**, 110601 (2023).
- [13] K. Sugisaki, T. Kato, Y. Minato, K. Okuwaki, and Y. Mochizuki, *Phys. Chem. Chem. Phys.* **24**, 8439 (2022).
- [14] S. Guo *et al.*, *Nat. Phys.* **20**, 1240 (2024).
- [15] M. Ostaszewski, E. Grant, and M. Benedetti, *Quantum* **5**, 391 (2021).
- [16] H. L. Tang, V. Shkolnikov, G. S. Barron, H. R. Grimsley, N. J. Mayhall, E. Barnes, and S. E. Economou, *PRX Quantum* **2**, 020310 (2021).
- [17] R. Villela, V. S. Prasanna, and B. P. Das, *Eur. Phys. J. Plus* **137**, 1017 (2022).
- [18] K. Sugisaki, K. Toyota, K. Sato, D. Shiomi, and T. Takui, *J. Phys. Chem. Lett.* **12**, 2880 (2021).
- [19] Sumeet, S. Prasanna V, B. P. Das, and B. K. Sahoo, *Quantum Rep.* **4**, 173 (2022).
- [20] K. Bharti *et al.*, *Rev. Mod. Phys.* **94**, 015004 (2022).
- [21] M. Motta and J. E. Rice, *Wiley Interdiscip. Rev. Comput. Mol. Sci.* **12**, e1580 (2022).
- [22] P. Chawla *et al.*, arXiv preprint physics.atom-ph/2406.04992 (2024).
- [23] K. Sugisaki, T. Kato, Y. Minato, K. Okuwaki, and Y. Mochizuki, *Phys. Chem. Chem. Phys.* **24**, 8439 (2022).
- [24] D. Halder, V. S. Prasanna, and R. Maitra, *J. Chem. Phys.* **157**, 174117 (2022).
- [25] D. Halder, V. S. Prasanna, V. Agarawal, and R. Maitra, *Int. J. Quantum Chem.* **123**, e27021 (2023).
- [26] I. O. Sokolov, P. K. Barkoutsos, P. J. Ollitrault, D. Greenberg, J. Rice, M. Pistoia, and I. Tavernelli, *J. Chem. Phys.* **152**, 124107 (2020).
- [27] F. Pavosevic, I. Tavernelli, and A. Rubio, *J. Phys. Chem. Lett.* **14**, 7876 (2023).
- [28] M. Rossmannek, F. Pavosevic, A. Rubio, and I. Taver-

- nelly, J. Phys. Chem. Lett. **14**, 3491 (2023).
- [29] J. Paldus, P. Piecuch, L. Pylypow, and B. Jeziorski, Phys. Rev. A **47**, 2738 (1993).
- [30] G. M. J. Barca *et al.*, J. Chem. Phys. **152**, 154102 (2022).
- [31] T. Kadowaki and H. Nishimori, Phys. Rev. E **58**, 5355 (1998).
- [32] T. Kadowaki, arXiv preprint quant-ph/0205020 (2002).
- [33] E. Farhi, J. Goldstone, S. Gutmann, and M. Sipser, arXiv preprint quant-ph/0001106 (2000).
- [34] M. Born and F. Vladimir, Z. Phys. **51**, 10.1007/BF01343193 (1928).
- [35] Fan, P. Dong, and P. Piecuch, Adv. Quantum Chem. **51**, 1 (2015).
- [36] J. Hubbard, Math. Phys. Sci. **276**, 238 (1963).
- [37] J. Dukelsky, G. Dussel, J. G. Hirsch, and P. Schuck, Nucl. Phys. A **714**, 63 (2003).
- [38] T. Henderson, J. Dukelsky, E. Gustavo, A. Signoracci, and T. Duguet, Phys. Rev. C **89**, 63 (2014).
- [39] J. von Neumann and E. P. Wigner, Phys. Z **30** (1929).
- [40] dwavesystems, dwave-samplers (2024), accessed: 2024-12-12.
- [41] D. Halder, V. S. Prasanna, and R. Maitra, J. Chem. Phys. **157**, 174117 (2022).
- [42] W. Lechner, P. Hauke, and P. Zoller, Sci. Adv. **1**, 10.1126/SCI-ADV.1500838/SUPPL_FILE/1500838_SM.PDF (2015).
- [43] A. Javadi-Abhari, M. Treinish, K. Krsulich, C. J. Wood, J. Lishman, J. Gacon, S. Martiel, P. D. Nation, L. S. Bishop, A. W. Cross, B. R. Johnson, and J. M. Gambetta, Quantum computing with Qiskit (2024), arXiv:2405.08810 [quant-ph].
- [44] P. J. Ollitrault *et al.*, Phys. Rev. Research **2**, 043140 (2020).
- [45] Y. Atobe, M. Tawada, and N. Togawa, IEEE Transactions on Computers **71**, 2606 (2022).